



Effect of hybrid nanoinks on solution-based Sn-doped In₂O₃ films under low-temperature microwave annealing

Bon-Ryul Koo, Hyo-Jin Ahn*

Department of Materials Science and Engineering, Seoul National University of Science and Technology, Seoul 139-743, Korea

Received 6 August 2015; received in revised form 20 August 2015; accepted 21 August 2015

Available online 2 September 2015

Abstract

Solution-based Sn-doped In₂O₃ (ITO) films were fabricated using well-dispersed hybrid ITO nanoinks, which consisted of high-crystalline ITO nanoparticles and ITO sols, by combining the methods of spin-coating and low-temperature microwave annealing. To investigate the optimum conditions for the hybrid ITO nanoinks, we used four different weight ratios of ITO nanoparticles to ITO sols in the hybrid nanoinks: 0 (sample A), 0.06 (sample B), 0.12 (sample C), and 0.24 (sample D). Sample D exhibited superior sheet resistance ($\sim 131.3 \Omega/\square$), good transmittance ($\sim 87.2\%$), and excellent figure of merit ($\sim 19.3 \times 10^{-4} \Omega^{-1}$) when compared to the other samples. This improvement performance is due to the improved densification of the solution-based ITO films, where the optimum amount of ITO sols in the films served as a smooth medium that linked the high-crystalline ITO nanoparticles. Therefore, our study can offer a novel strategy that can be applied to flexible transparent conducting films (TCFs) as well as to the low-cost fabrication of high-performance TCFs in various optoelectronic applications.

© 2015 Elsevier Ltd and Techna Group S.r.l. All rights reserved.

Keywords: A. Films; C. Electrical properties; C. Optical properties; Solution-based Sn-doped In₂O₃; Nanoinks

1. Introduction

Transparent conducting films (TCFs) with low resistivities ($< 10^{-3} \Omega \text{ cm}$) and high transmittances ($> 80\%$) are critical for various optoelectronic devices, including solar cells, liquid crystal displays (LCDs), light emitting diodes (LEDs), and touch screens [1–4]. Among the various TCF materials (In₂O₃:Sn (ITO), SnO₂:F (FTO), ZnO:Al (AZO), and SnO₂:Sb (ATO)), ITO, which is conventionally prepared by various vacuum-based deposition processes, such as RF magnetron-sputtering, vacuum evaporation, and chemical vapor deposition, has the best conductivity and a high transparency [5–7]. Until now, most studies have mainly focused on using vacuum-based processes, like the above-mentioned methods, to obtain high-performance ITO films. For the vacuum-based process, the high vacuum conditions ($< 10^{-4} \text{ Pa}$) and sophisticated equipment are required, which contributes to the high cost of ITO films

and limits its broad industrial applicability [2]. Recently, in order to replace this vacuum-based process, researchers have proposed various solution-based processes [8]. In particular, because a solution-based process would not require a vacuum atmosphere or sophisticated equipment, it enables the fabrication of ITO films at a low cost and larger scale [9]. In addition, various solution-based processes, such as inkjet-printing, dip-coating, and spin-coating, have been developed to fabricate solution-based ITO films [1,10,11]. For example, Jeong et al. fabricated ITO films by ink-jet printing followed by rapid thermal annealing and obtained a sheet resistance of $\sim 202.7 \Omega/\square$ and an optical transmittance of $\sim 88.0\%$ at a calcination temperature of $\sim 450 \text{ }^\circ\text{C}$ [1]. Kőrösi et al. reported that an ITO film with an optimized thickness, which was achieved by repetitive dip-coating, exhibited a sheet resistance of $\sim 3.6 \text{ k}\Omega/\square$ and an optical transmittance of $\sim 66.3\%$ after calcination at $550 \text{ }^\circ\text{C}$ [10]. Sunde et al. prepared ITO films by spin-coating crystalline ITO nanoparticles and achieved a sheet resistance of $\sim 270.0 \Omega/\square$ and a transmittance of $\sim 80.0\%$ at an annealing temperature of $\sim 530 \text{ }^\circ\text{C}$ [11].

*Corresponding author. Tel.: +82 29706622; fax: +82 29736657.

E-mail address: hjahn@seoultech.ac.kr (H.-J. Ahn).

Hwang et al. reported that the inkjet-printed ITO films prepared using a microwave annealing exhibited a sheet resistance of $\sim 517.0 \Omega/\square$ and optical transmittance of $\sim 87.0\%$ at an annealing temperature of 400°C [12]. Hong et al. prepared the inkjet-printed ITO films by adjusting the heat-treatment conditions and proposed an optimized sheet resistance of $\sim 455.0 \Omega/\square$ and transmittance $\sim 90.0\%$ at 600°C under a N_2 atmosphere [13]. However, to synthesize ITO films with excellent electrical and optical properties using solution-based methods, high annealing temperatures are required, which decreases its price competitiveness for fabricating high-performance TCFs and has side effects that prevent its use in diverse applications such as flexible devices. Therefore, improving the performance of solution-based ITO films that are obtained at a low annealing temperature of 250°C would allow for the use of these films in various optoelectronic applications with advantages such as high flexibility and low fabrication costs.

In this work, we fabricated solution-based ITO films using hybrid nanoinks consisting of ITO nanoparticles and ITO sols by means of low-temperature microwave annealing at 250°C . This microwave-annealing method could improve the performance of solution-based ITO films even at a low annealing temperature because the internal heating system that is induced by absorbing microwaves can offer higher energy efficiencies (more than 80%) than a conventional electric furnace (less than 30%) [14].

2. Material and methods

The solution-based ITO films were fabricated using hybrid nanoinks by combining the methods of spin-coating and low-temperature microwave annealing. First, a precursor solution of indium (III) chloride tetrahydrate ($\text{InCl}_3 \cdot 4\text{H}_2\text{O}$, Aldrich) and tin (IV) chloride pentahydrate ($\text{SnCl}_4 \cdot 5\text{H}_2\text{O}$, Aldrich) were dissolved in de-ionized (DI) water in order to synthesize the ITO nanoparticles using co-precipitation. The optimum molar ratio of In:Sn was adjusted to 9:1, as previously reported [15]. Next, ammonium water (NH_4OH , Duksan) was added into the above-prepared solution while stirring until the $\text{pH}=6.75$ to obtain ITO nanoparticles with the lowest resistivity were reached [16]. At this time, white indium tin hydroxides precipitated in the solution. The resulting precipitation was centrifuged at 3000 rpm for 5 min and washed several times with DI water in order to remove the residual reactants such as the ammonia and chloride components. The pure indium tin hydroxides that were collected were dried at 50°C and microwave-annealed at 700°C for 5 min in air in order to obtain high-crystalline ITO nanoparticles. The microwave annealing resulted in the formation of ITO nanoparticles with high crystallinity because it has a higher annealing efficiency than conventional thermal processes [14]. To make hybrid nanoinks with the ITO sols, indium (III) chloride tetrahydrate and tin (II) chloride dihydrate ($\text{SnCl}_2 \cdot 2\text{H}_2\text{O}$, Aldrich) were dissolved in 2-propanol [$(\text{CH}_3)_2\text{CHOH}$, Aldrich], with the above-mentioned optimum molar ratio of In:Sn. Next, the obtained ITO nanoparticles were mixed with the ITO sols, which were spin-coated onto the glass substrate

at 2000 rpm for 30 s. To investigate the optimum conditions for the solution-based ITO films fabricated at a low temperature of 250°C , the weight ratios of ITO nanoparticles to ITO sols in the hybrid nanoinks were controlled to 0, 0.06, 0.12, and 0.24 (referred to hereafter as sample A, sample B, sample C, and sample D, respectively). The as-prepared ITO films were dried at 150°C for 3 h in a convection oven and then microwave-annealed at 250°C for 5 min in an argon atmosphere. Finally, we obtained solution-based ITO films by combining the methods of spin-coating and low-temperature microwave annealing.

The surface morphology and topology of the as-prepared ITO films were examined using field-emission scanning electron microscopy (FE-SEM, Hitachi S-4800) and atomic force microscopy (AFM, diDimension™ 3100). The structural analysis of the samples was carried out using multifunctional transmission electron microscopy (MULTI/TEM; Tecnai G², Gwangju Center). The crystalline structure and chemical bonding states of the ITO films were investigated using X-ray diffraction (XRD, Rigaku D/Max-2500 diffractometer using $\text{Cu K}\alpha$ radiation) and X-ray photoelectron spectroscopy (XPS, ESCALAB 250 equipped with an $\text{Al K}\alpha$ X-ray source), respectively. The electrical and optical properties of all of the samples were investigated using a Hall effect measurement system (Ecopia, HMS-3000) and ultraviolet–visible (UV–vis) spectroscopy (Perkim-Elmer Lambda-35).

3. Results and discussion

Hybrid ITO nanoinks were prepared by a mixture of ITO nanoparticles and ITO sols consisting of In and Sn ions dissolved in 2-propanol, as shown in Fig. 1(a). We believe

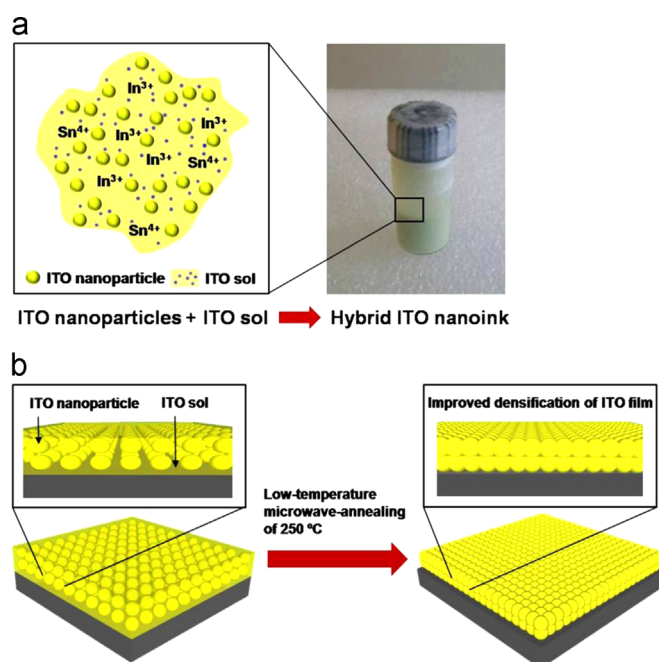


Fig. 1. A schematic for (a) hybrid ITO nanoinks consisting of high-crystalline ITO nanoparticles and ITO sols and (b) solution-based ITO films using a low-temperature microwave annealing.

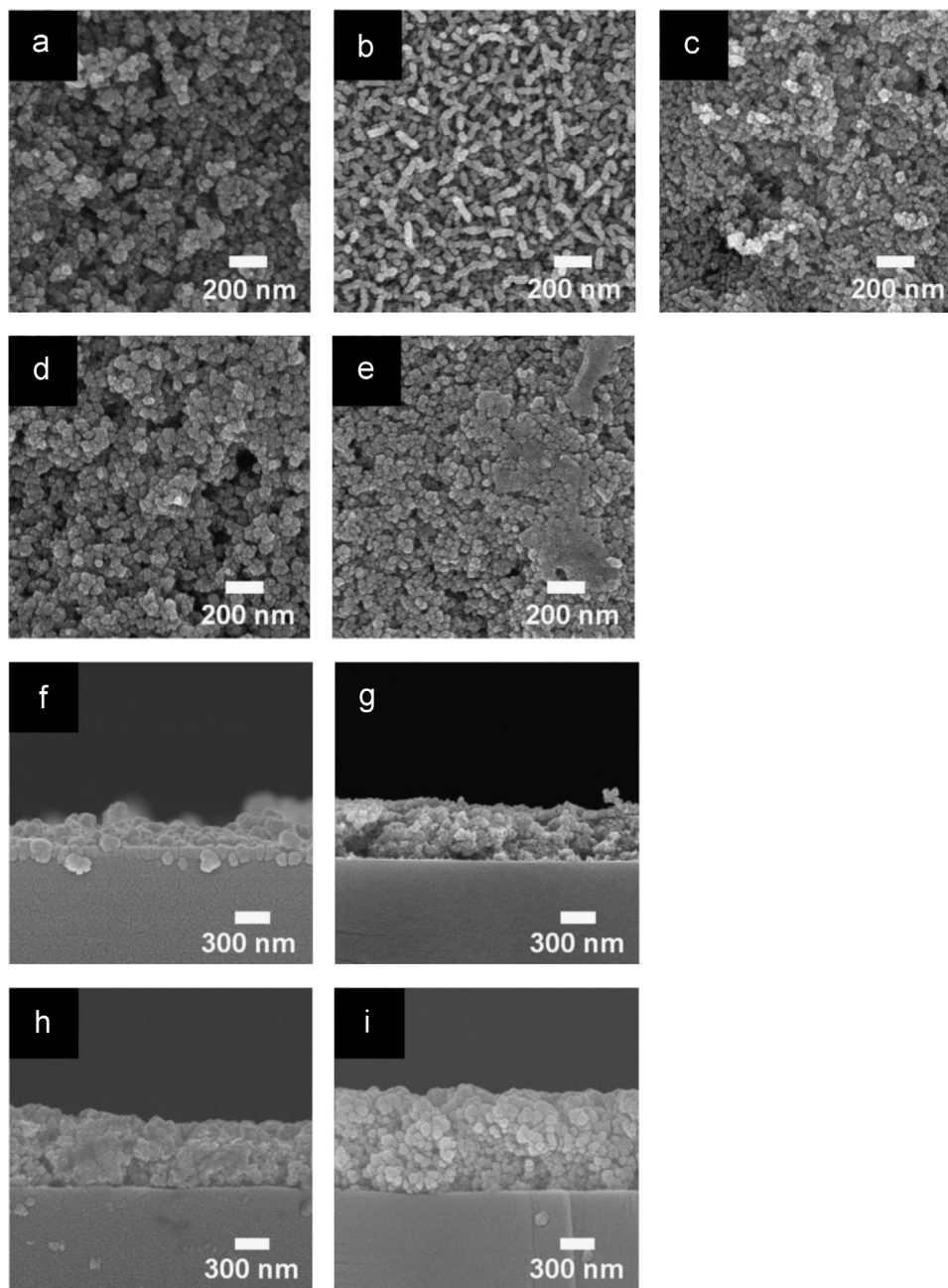


Fig. 2. (a–e) Top-view FE-SEM images of the ITO nanoparticles alone and samples A–D. (f–i) Cross-section FE-SEM images of samples A–D.

that hybrid ITO nanoinks have excellent dispersibility when compared to ITO nanoinks without ITO sols. In general, ITO nanoparticles that are in a solvent are easily agglomerated by attractive van der Waals forces [17]. However, in order to improve their dispersibility, additives are absorbed on the nanoparticles, which results in repulsive forces that prevent other nanoparticles from coming into close proximity [18]. Hence, the addition of a dispersing agent allowed the ITO nanoinks to remain stable without agglomeration. In particular, in the hybrid ITO nanoinks, the ITO sols serve as the dispersing agent, which can improve the dispersibility of the ITO nanoparticles. Fig. 1(b) presents a schematic of the solution-based ITO films fabricated using a low-temperature microwave method. After spin-coating of the hybrid ITO

nanoinks, the samples were microwave-annealed at 250 °C in order to synthesize the solution-based ITO films. During this process, the ITO sols play an important role in the smooth medium that connects the ITO nanoparticles resulting in improved densification of the solution-based ITO films.

Fig. 2(a)–(e) show the top-view FE-SEM images of the ITO nanoparticles alone, sample A, sample B, sample C, and sample D, respectively. As shown in Fig. 2(a), the ITO nanoparticles exhibit irregular morphologies and their diameter is in the range of ~16.7 to ~47.5 nm. Sample A (Fig. 2(b)) was prepared using only ITO sols and the surface of the ITO film is rough and discontinuous. We expected to form ITO films with dense and uniform surfaces; however, the rough and discontinuous surface of sample A was formed because of the

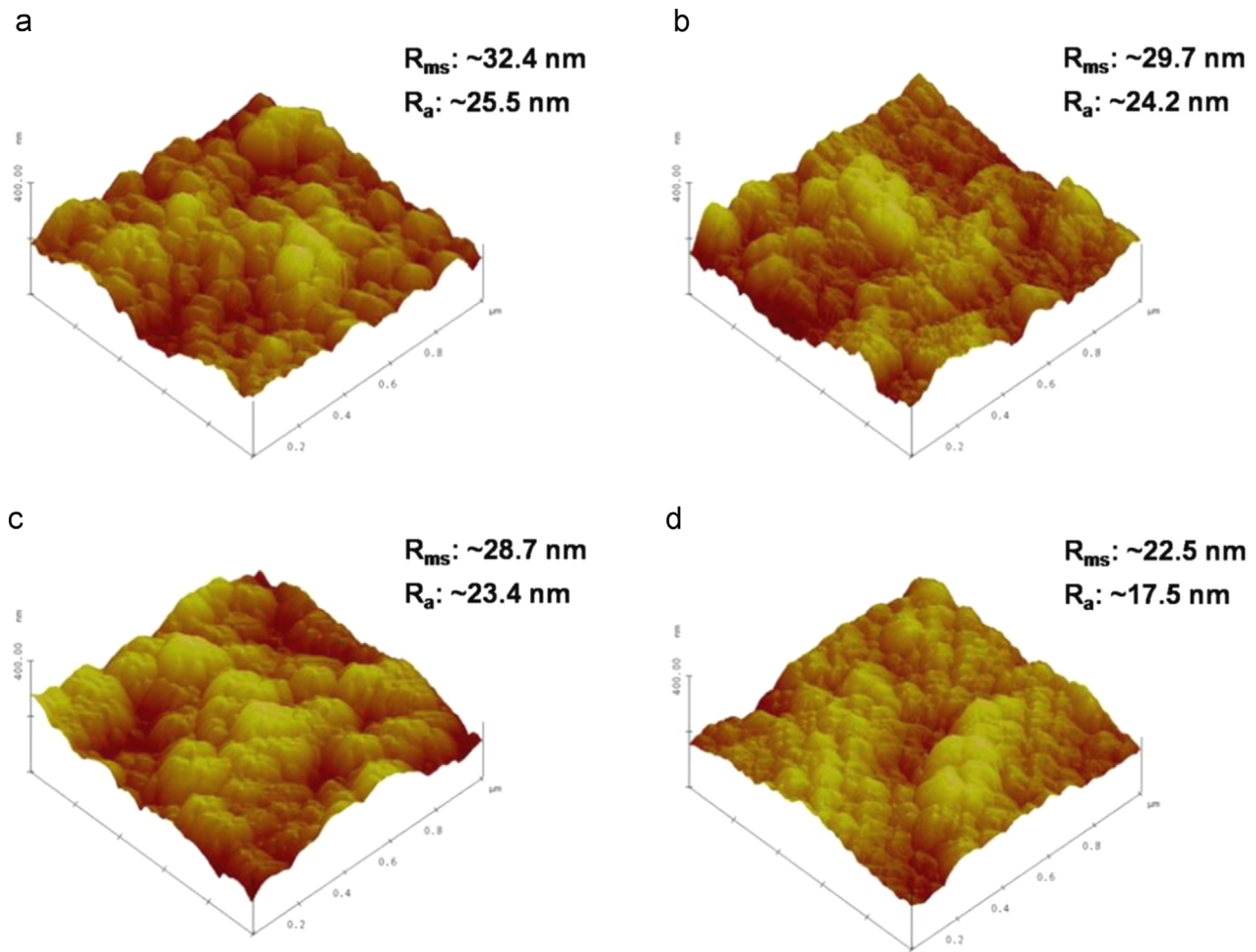


Fig. 3. AFM images obtained from (a) sample A, (b) sample B, (c) sample C, and (d) sample D.

fast ITO grain growth during microwave annealing, which has a high energy efficiency despite a low temperature of 250 °C [16]. Thus, sample A, with its rough surface, can offer a high sheet resistance due to the increase in electron scattering at its grain boundaries [19]. For the samples prepared with the hybrid nanoinks, the surface morphologies gradually changed from a rough surface to a dense surface as the weight ratio of ITO nanoparticles to ITO sols increased. As a result, while sample B generated grain growth due to the relatively large amount of ITO sols, sample D resulted in enhanced surface densification due to the relatively large amount of ITO nanoparticles. It should be noted that the diameter of sample D (~28.0–63.6 nm) was slightly larger than the ITO nanoparticles. As an explanation for this result, the ITO sols in the solution-based ITO films play a key role as a matrix for the ITO films as well as a glue to improve the connection between ITO nanoparticles during the microwave-annealing process. As shown in Fig. 2(f)–(i), the average thickness of the samples was ~311.7 nm for sample A, ~447.6 nm for sample B, ~609.2 nm for sample C, and ~877.6 nm for sample D. Therefore, the thickness of the solution-based ITO films gradually increases as the weight ratio of ITO nanoparticles to ITO sols increases. Furthermore, the cross-sectional FESEM image of sample D shows that it has a relatively high packing

density without voids when compared to the other samples. Therefore, the high densification of the solution-based ITO films can affect its electrical properties [20].

To further investigate the surface roughness of the solution-based ITO films, AFM measurements were carried out. Fig. 3 (a)–(d) shows the AFM images obtained from samples A–D. The root mean square roughness (R_{ms}) is defined as the standard deviation of the height in a given surface area and the height roughness (R_a) is the average value of the surface height in proportion to the center plane, which correspond to the interface width and the height roughness, respectively [21]. These factors directly affect the electrical properties of the solution-based ITO films. In particular, decreasing the surface roughness is important in order to enhance the electrical properties of the solution-based ITO films. The R_{ms} and R_a of the solution-based ITO films were ~32.4 nm and ~25.5 for sample A, ~29.7 nm and ~24.2 for sample B, ~28.7 nm and ~23.4 for sample C, ~22.5 nm and ~17.5 for sample D, respectively. It can be seen that the interface width and the height roughness decreased as the weight ratio of ITO nanoparticles to ITO sols increased in the hybrid nanoinks. As a result, sample D had the optimized weight ratio of ITO nanoparticles to ITO sols, which offered a short distance and smooth connections between the ITO nanoparticles, resulting

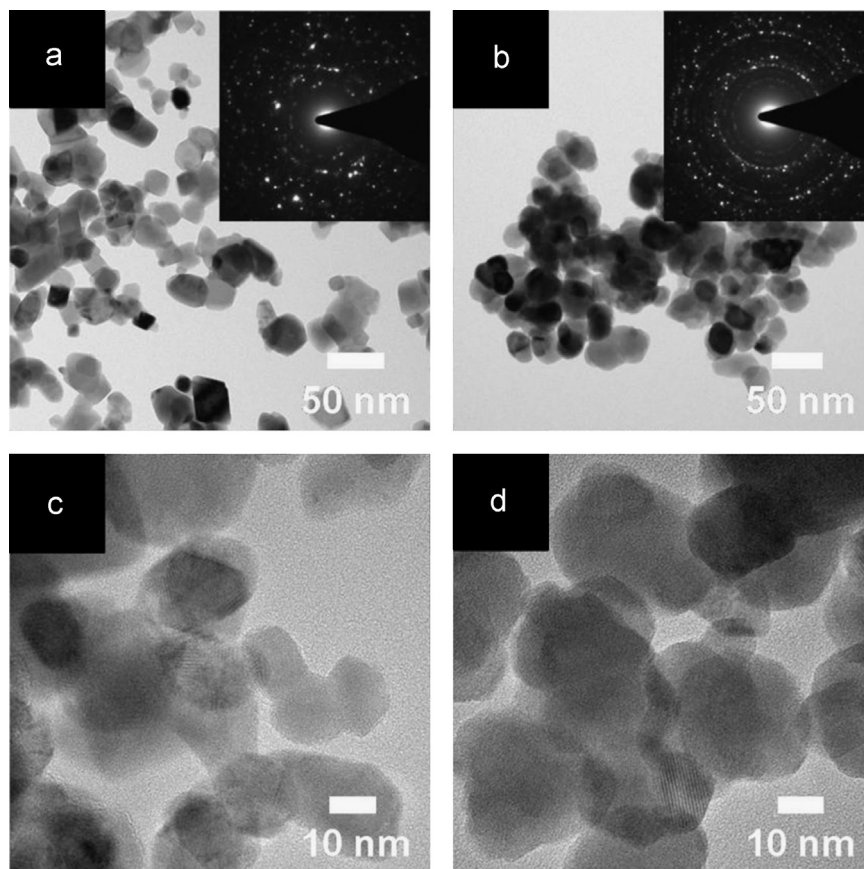


Fig. 4. (a–b) TEM images and (c–d) high-resolution TEM images obtained from the ITO nanoparticles alone and from sample D. The insets show SAED patterns obtained from the ITO nanoparticles alone and sample D.

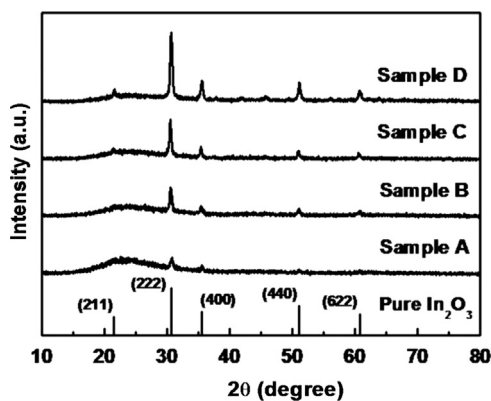


Fig. 5. X-ray diffraction patterns of sample A, sample B, sample C, and sample D.

in decreased electron scattering at the ITO nanoparticle interfaces [22]. Thus, the solution-based ITO film of sample D exhibited a uniform and dense surface when compared to the other samples.

Fig. 4(a)–(d) shows the TEM images and high-resolution TEM images obtained from the ITO nanoparticles alone and from sample D. Fig. 4(a) shows the irregular morphology of the ITO nanoparticles, which were ~ 15.8 – 45.5 nm in diameter. In addition, most of the ITO nanoparticles were distributed independent of each other without interconnections. On the other hand, sample D, which was obtained using the

hybrid nanoinks, showed that most of the ITO nanoparticles were continuously linked. The selected area electron diffraction (SAED) patterns (the insets of Fig. 4(a) and (b)) of the ITO nanoparticles alone, which are shown in Fig. 4(a), exhibit strong spot patterns; however, sample D simultaneously presents spot and ring patterns, which means that it consists of both high-crystalline ITO nanoparticles prepared at a high annealing temperature of 700 °C and a relatively low-crystalline ITO phases that was formed at a low microwave-annealing temperature of 250 °C. As shown in Fig. 4(c) and (d), the ITO nanoparticles of sample D (~ 24.5 – 60.6 nm) increased slightly in diameter compared to those prepared by co-precipitation because of the existence of ITO sols in the hybrid nanoinks. These results prove that the existence of the ITO sols in the hybrid nanoinks acts like a glue that forms connections between the ITO nanoparticles, resulting in the successful formation of high-performance solution-based ITO films despite the use of a low annealing temperature of 250 °C.

Fig. 5 shows the XRD patterns of all of the samples obtained after microwave-annealing at 250 °C. All of the samples present broad peaks around 23° , which correspond to a glass substrate (Corning EAGLE XG™) with amorphous characteristics. In comparison with the XRD pattern of pure In_2O_3 , the main characteristic diffraction peaks of all of the samples resemble those of the polycrystalline In_2O_3 with a cubic bixbyite structure (space group $1a3$ [206]; JCPDS card no. 06-0416). The intensive peaks observed at 30.66° and

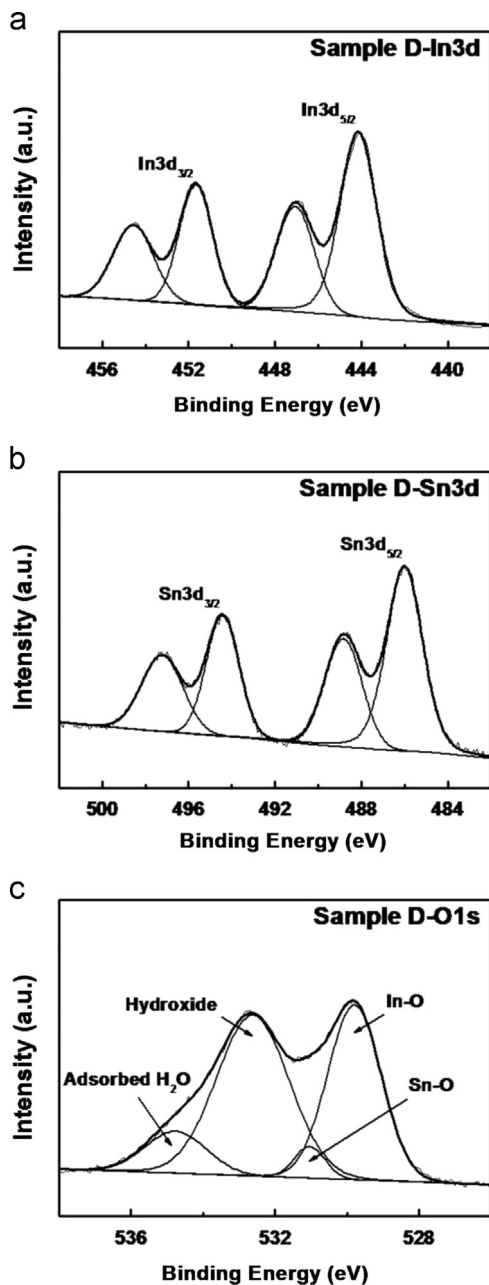


Fig. 6. XPS core-level spectra of (a) In 3d, (b) Sn 3d, and (c) O 1s obtained from sample D.

35.54° are indexed to the (222) and (400) planes. The position of these peaks is slightly shifted towards higher diffraction angles compared to those of pure In_2O_3 . This suggests the successful formation of the ITO phase by the doping of Sn^{4+} into the In_2O_3 lattice because the ionic radius of Sn^{4+} (0.69 Å) is smaller than that of In^{3+} (0.80 Å), which can be explained using Bragg's equation ($n\lambda = 2d \sin\theta$) [14,23]. In addition, the peak intensity of the samples gradually increased as the relative amount of ITO nanoparticles increased in the hybrid nanoinks, which is caused by the increased thickness of the solution-based ITO films. Thus, the XRD results confirm the successful synthesis of solution-based ITO films using low-temperature microwave-annealing at 250°C .

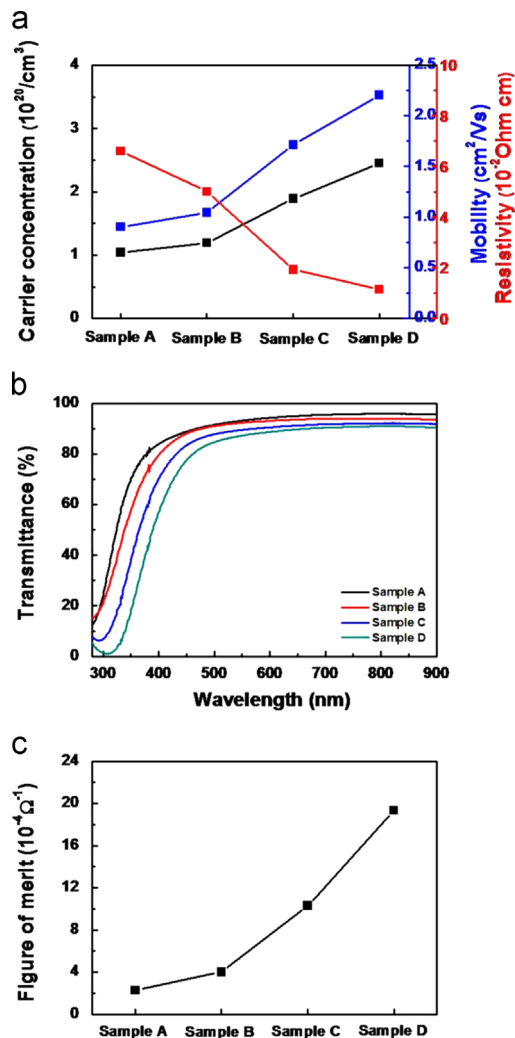


Fig. 7. (a) Electrical properties, (b) optical transmission spectra, and (c) figure of merit (FOM) obtained from all of the samples.

To investigate the chemical binding states of elemental In, Sn, and O in sample D, XPS analyses were performed as shown in Fig. 6(a)–(c). All of the binding energies were adjusted by referencing the C 1s of 284.5 eV. The main peaks of In $3d_{5/2}$ and In $3d_{3/2}$ photoelectrons were observed at ~ 444.1 eV and ~ 451.6 eV, respectively, indicating that elemental In exists as In^{3+} ions in the In_2O_3 phases. For the Sn $3d_{5/2}$ and Sn $3d_{3/2}$ photoelectrons shown in Fig. 6(b), dominant peaks were observed at ~ 485.9 eV and ~ 494.4 eV, respectively, corresponding to the existence of Sn^{4+} ions in the SnO_2 phases. Thus, Sn^{4+} ions act as donors in the In_2O_3 lattices, implying that Sn-doped In_2O_3 phases are successfully formed [14]. Furthermore, additional peaks were observed at ~ 447.0 eV and ~ 454.5 eV for In 3d and ~ 488.8 eV and ~ 497.2 eV for Sn 3d, indicating the existence of indium hydroxide and tin hydroxide, respectively [24,25]. In general, $\text{In}(\text{OH})_3$ and $\text{Sn}(\text{OH})_4$ undergo phase transformations to In_2O_3 and SnO_2 , respectively, at annealing temperatures higher than $\sim 330^\circ\text{C}$ [26,27]. Thus, indium hydroxide and tin hydroxide are observed on the ITO films due to low-temperature microwave annealing at 250°C . These results are confirmed

in the XPS spectra of the O 1s photoelectron in Fig. 6(c). The XPS spectra of O 1s consist of four peaks at ~ 529.7 eV, ~ 531.0 eV, ~ 532.6 eV, and ~ 534.7 eV, corresponding to the phases related to In–O, Sn–O, hydroxide, and H₂O adsorbed on the surface, respectively [14,28]. Herein, the XPS results indicate that In-hydroxide states are present on the surface of the solution-based ITO films and are hypothesized to be formed during the low-temperature microwave annealing process. The FE-SEM, TEM, XRD, and XPS results prove the successful formation of the solution-based ITO films using low-temperature microwave-annealing at 250 °C.

Fig. 7(a) displays the electrical properties of the samples, such as the carrier concentrations, Hall mobilities, and resistivities. The carrier concentrations gradually increase from $\sim 1.04 \times 10^{20} \text{ cm}^{-3}$ for sample A to $\sim 2.45 \times 10^{20} \text{ cm}^{-3}$ for sample D. This is owing to the increase in thickness of the solution-based ITO films as the amount of ITO nanoparticles in the hybrid nanoinks increased. The Hall mobilities of the samples were measured to be $\sim 0.90 \text{ cm}^2/(\text{V s})$ for sample A, $\sim 1.04 \text{ cm}^2/(\text{V s})$ for sample B, $\sim 1.71 \text{ cm}^2/(\text{V s})$ for sample C, and $\sim 2.20 \text{ cm}^2/(\text{V s})$ for sample D. Sample D has the highest Hall mobility owing to the improved densification of its solution-based ITO films. Therefore, the resistivity (ρ) of the samples can be calculated using the carrier concentration (N) and Hall mobility (μ) using the following equation [14,19]:

$$\rho = 1/(Ne\mu) \quad (2)$$

where N is the carrier concentration, e is the electron charge ($1.602 \times 10^{-19} \text{ C}$), and μ is the Hall mobility. Thus, the resistivities (ρ) of the films were calculated to be $\sim 6.60 \times 10^{-2} \Omega \text{ cm}$ for sample A, $\sim 5.01 \times 10^{-2} \Omega \text{ cm}$ for sample B, $\sim 1.92 \times 10^{-2} \Omega \text{ cm}$ for sample C, and $\sim 1.15 \times 10^{-2} \Omega \text{ cm}$ for sample D. In addition, the sheet resistances, i.e., the resistivity/thickness of the ITO films, were observed to be $\sim 2128 \Omega/\square$ for sample A, $\sim 1120 \Omega/\square$ for sample B, $\sim 316.4 \Omega/\square$ for sample C, and $\sim 131.3 \Omega/\square$ for sample D. Therefore, sample D showed excellent electrical properties compared to the other samples despite a low annealing temperature of 250 °C. This result is due to the enhanced densification of the solution-based ITO films, which results in smooth linkages between the high-crystalline ITO nanoparticles when an optimized weight ratio of ITO nanoparticles to ITO sols in the hybrid nanoinks is used. Fig. 7(b) presents the optical transmittances obtained for samples A–D. In general, the optical transmittances at 550 nm gradually

decreased as the thickness of the solution-based TCFs increased. However, for the solution-based ITO films using hybrid ITO nanoinks, in spite of the dramatic increase in the thickness of the ITO films, the transmittance decreased slightly owing to the decrease in light scattering that resulted in improved densification of the ITO films [29]. Furthermore, Table 1 shows the electrical and optical properties of ITO films obtained from various solution-based processes as well as from our works. Solution-based ITO films have been fabricated using various processes as reported previously, such as inkjet-printing, dip coating, and spin coating [1,10–12,29–31]. These methods demand high-temperature annealing processes (300–550 °C) in order to improve the performances of the solution-based ITO films. However, in this study, the solution-based ITO films that were prepared using hybrid ITO nanoinks show excellent electrical and optical properties despite a low annealing temperature of 250 °C when compared to previously reported works, as shown in Table 2. To investigate the comprehensive quality of the TCFs, the figure of merit (FOM) can be calculated using the following equation [19]:

$$\text{FOM} = T^{10}/R_s$$

where T is the transmittance of the films and R_s is the sheet resistance. The FOM values were calculated to be $\sim 2.3 \times 10^{-4} \Omega^{-1}$ for sample A, $\sim 4.0 \times 10^{-4} \Omega^{-1}$ for sample B, $\sim 10.3 \times 10^{-4} \Omega^{-1}$ for sample C, and $\sim 19.3 \times 10^{-4} \Omega^{-1}$ for sample D. Generally, the higher the FOM, the better is the performance of TCFs. As such, sample D exhibited the best TCF performance because it had both a low sheet resistance ($\sim 131.3 \Omega/\square$) and a good transmittance ($\sim 87.2\%$). Thus, solution-based ITO films fabricated from hybrid nanoinks using low-temperature microwave annealing were developed and can be potentially used flexible optoelectronic applications as well as low fabrication cost of TCFs.

4. Conclusions

We fabricated solution-based ITO films from hybrid nanoinks by combining the methods of spin-coating and low-temperature microwave annealing. Hybrid ITO nanoinks consisting of high-crystalline ITO nanoparticles and ITO sols have excellent dispersibility due to the existence of In and Sn ions, which act as dispersing agents. To investigate the optimum conditions for the hybrid nanoinks, we adjusted the weight ratios of ITO nanoparticles to ITO sols that were used

Table 1

List of electrical and optical properties for the solution-based ITO films obtained from various solution-based processes.

Processes	Sheet resistance (Ω/\square)	Transmittance (% , at 550 nm)	Annealing temperature (°C)	References
Inkjet-printing	~ 202	~ 88	450	[1]
Inkjet-printing	~ 517	~ 87	400	[28]
Dip-coating	$\sim 3.6 \times 10^3$	~ 66	550	[10]
Dip-coating	$\sim 7.0 \times 10^3$	~ 83	500	[29]
Spin-coating	~ 270	~ 80	530	[11]
Spin-coating	~ 133	~ 88	300	[12]
Spin-coating + microwave annealing	~ 131	~ 87	250	our works

Table 2
Summary of electrical and optical properties obtained from samples A–D.

	Sample A	Sample B	Sample C	Sample D
Carrier concentration (cm^{-3})	1.04×10^{20}	1.19×10^{20}	1.89×10^{20}	2.45×10^{20}
Hall mobility ($\text{cm}^2/(\text{V s})$)	0.90	1.04	1.71	2.20
Resistivity ($\Omega \text{ cm}$)	6.60×10^{-2}	5.01×10^{-2}	1.92×10^{-2}	1.15×10^{-2}
Sheet resistance (Ω/\square)	2128	1120	316.4	131.3
Transmittance (% , at 550 nm)	93.1	92.3	89.4	87.2

in the hybrid nanoinks as: 0 (sample A), 0.06 (sample B), 0.12 (sample C), and 0.24 (sample D). In particular, sample D exhibited an excellent sheet resistance ($\sim 131.3 \Omega/\square$), good transmittance ($\sim 87.2\%$), and superior FOM ($\sim 19.3 \times 10^{-4} \Omega^{-1}$) despite the use of a low annealing temperature of 250°C . This improvement in performance was attributed to the improved densification of the solution-based ITO films fabricated from the optimized hybrid nanoinks using low-temperature microwave annealing. The improved densification occurred because the high-crystalline ITO nanoparticles were smoothly connected by the ITO sol that was used in the hybrid nanoinks. Thus, the solution-based ITO films that were fabricated from the hybrid nanoinks by low-temperature microwave annealing may be an attractive candidate for use as potential TCFs in optoelectronic applications that require the use of low-temperature fabrication.

Acknowledgments

This work was supported by Grant no. 10041161 from the Ministry of Knowledge Economy (MKE) and the Fundamental R&D Program for Core Technology of Materials funded by the Ministry of Knowledge Economy, Republic of Korea.

References

- [1] J.-A. Jeong, J. Lee, H. Kim, H.-K. Kim, S.-I. Na, Ink-jet printed transparent electrode using nano-size indium tin oxide particles for organic photovoltaics, *Sol. Energy Mater. Sol. Cells* 94 (2010) 1840–1844.
- [2] C.J. Brabec, Organic photovoltaics: technology and market, *Sol. Energy Mater. Sol. Cells* 83 (2004) 273–292.
- [3] N. Ameera, A. Shuhaimi, N. Surani, M. Rusop, M. Hakim, M.H. Mamat, M. Mansor, M. Sobri, V. Ganesh, Y. Yusuf, Nanocolumnar zinc oxide as a transparent conductive film for a blue InGaN-based light emitting diode, *Ceram. Int.* 41 (2015) 913–920.
- [4] H.-K. Kim, S. Lee, K.-S. Yun, Capacitive tactile sensor array for touch screen application, *Sens. Actuators A* 165 (2011) 2–7.
- [5] K.C. Heo, Y. Sohn, J.S. Gwag, Effects of an additional magnetic field in ITO thin film deposition by magnetron sputtering, *Ceram. Int.* 41 (2015) 617–621.
- [6] J.K. Sheu, Y.K. Su, G.-C. Chi, M.J. Jou, C.M. Chang, Effects of thermal annealing on the indium tin oxide Schottky contacts of n-GaN, *Appl. Phys. Lett.* 72 (1998) 3317–3319.
- [7] T. Maruyama, K. Fukui, Indium-tin oxide thin films prepared by chemical vapor deposition, *J. Appl. Phys.* 70 (1991) 3848–3851.
- [8] Z. Chen, W. Li, R. Li, Y. Zhang, G. Xu, H. Cheng, Fabrication of highly transparent and conductive indium–tin oxide thin films with a high figure of merit via solution processing, *Langmuir* 29 (2013) 13836–13842.
- [9] R.M. Pasquarelli, D.S. Ginley, R. O’Hayre, Solution processing of transparent conductors: from flask to film, *Chem. Soc. Rev.* 40 (2011) 5406–5441.
- [10] L. Kőrösi, S. Papp, I. Dékány, Preparation of transparent conductive indium tin oxide thin films from nanocrystalline indium tin hydroxide by dip-coating method, *Thin Solid Films* 519 (2011) 3113–3118.
- [11] T.O.L. Sunde, E. Garskaite, B. Otter, H.E. Fosshiem, R. Saeterli, R. Holmestad, M.-A. Einarsrud, T. Grande, Transparent and conducting ITO thin films by spin coating of an aqueous precursor solution, *J. Mater. Chem.* 22 (2012) 15740–15749.
- [12] M.-S. Hwang, B.-Y. Jeong, J. Moon, S.-K. Chun, J. Kim, Inkjet-printing of indium tin oxide (ITO) films for transparent conducting electrodes, *Mater. Sci. Eng. B* 176 (2011) 1128–1131.
- [13] S.-J. Hong, J.-W. Kim, J.I. Han, Improvement of electrical properties of printed ITO thin films by heat-treatment conditions, *Curr. Appl. Phys.* 11 (2011) S202–S205.
- [14] M. Okuya, N. Ito, K. Shiozaki, ITO thin films prepared by a microwave heating, *Thin Solid Films* 515 (2007) 8656–8659.
- [15] B.-R. Koo, H.-J. Ahn, Surface modification and characterization of electrosprayed Sn-doped In_2O_3 thin films, *J. Nanosci. Nanotechnol.* 14 (2014) 9632–9636.
- [16] K.Y. Kim, S.B. Park, Preparation and property control of nano-sized indium tin oxide particle, *Mater. Chem. Phys.* 86 (2004) 210–221.
- [17] F.F. Lange, Powder processing science and technology for increased reliability, *J. Am. Ceram. Soc.* 72 (1989) 3–15.
- [18] J. Zhou, J. Ralston, R. Sedev, D.A. Beattie, Functionalized gold nanoparticles: synthesis, structure and colloid stability, *J. Colloid Interface Sci.* 331 (2009) 251–262.
- [19] H.-R. An, C.Y. Kim, S.-T. Oh, H.-J. Ahn, Effect of sol-layers on Sb-doped SnO_2 thin films as solution-based transparent conductive oxides, *Ceram. Int.* 40 (2014) 385–391.
- [20] T. Asikainen, M. Ritala, M. Leskelä, T. Prohaska, G. Friedbacher, M. Grasserbauer, AFM and STM studies on In_2O_3 and ITO thin films deposited by atomic layer epitaxy, *Appl. Surf. Sci.* 99 (1996) 91–98.
- [21] D. Raoufi, A. Kiasatpour, H.R. Fallah, A.S.H. Rozatian, Surface characterization and microstructure of ITO thin films at different annealing temperatures, *Appl. Surf. Sci.* 253 (2007) 9085–9090.
- [22] M. Higuchi, M. Sawada, Y. Kuronuma, Microstructure and electrical characteristics of sputtered indium tin oxide films, *J. Electrochem. Soc.* 140 (1993) 1773–1775.
- [23] J. Lee, S. Lee, G. Li, M.A. Petruska, D.C. Paine, S. Sun, A facile solution-phase approach to transparent and conducting ITO nanocrystal assemblies, *J. Am. Chem. Soc.* 134 (2012) 13410–13414.
- [24] T.P. Nguyen, P. Le Rendu, S.A. de Vos, An X-ray photoelectron spectroscopy investigation into the interface formed between poly(2-methoxy-5-(2-ethyl-hexyloxy)-*p*-phenylene vinylene) and indium tin oxide, *Synth. Metals* 138 (2003) 113–117.
- [25] T. Krishnakumar, R. Jayaprakash, N. Pinna, A.R. Phani, M. Passacantando, S. Santucci, Structural, optical, and electrical characterization of antimony-substituted tin oxide nanoparticles, *J. Phys. Chem. Solids* 70 (2009) 993–999.
- [26] N.C. Pramanik, S. Das, P.K. Biswas, The effect of Sn(IV) on transformation of co-precipitated hydrated In(III) and Sn(IV) hydroxides to indium tin oxide (ITO) powder, *Mater. Lett.* 56 (2002) 671–679.

- [27] G. Korotcenkov, V. Macsanov, V. Tolstoy, V. Brinzari, J. Schwank, G. Faglia, Structural and gas response characterization of nano-size SnO₂ films deposited by SILD method, *Sens. Actuators B* 96 (2003) 602–609.
- [28] A. Goudarzi, G.M. Aval, S.S. Park, M.-C. Choi, R. Sahraei, M.H. Ullah, A. Avane, C.-S. Ha, Low-temperature growth of nanocrystalline Mn-doped ZnS thin films prepared by chemical bath deposition and optical properties, *Chem. Mater.* 21 (2009) 2375–2385.
- [29] J. Liu, D. Wu, S. Zeng, Influence of temperature and layers on the characterization of ITO films, *J. Mater. Process. Technol.* 209 (2009) 3943–3948.
- [30] S.-J. Hong, J.-I. Han, Indium tin oxide (ITO) thin film fabricated by indium-tin-organic sol including ITO nanoparticle, *Curr. Appl. Phys.* 6S1 (2006) e206–e210.
- [31] J. Lee, M.A. Petruska, S. Sun, Surface modification and assembly of transparent indium tin oxide nanocrystals for enhanced conductivity, *J. Phys. Chem. C* 118 (2014) 12017–12021.